



Activated carbon made from cow dung as electrode material for electrochemical double layer capacitor



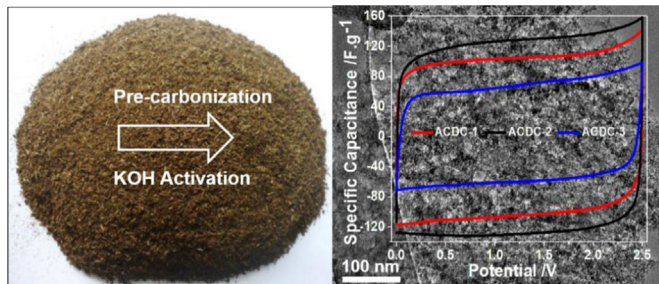
Dhrubajyoti Bhattacharjya, Jong-Sung Yu*

Department of Advanced Materials Chemistry, Korea University, 2511 Sejong-ro, Sejong City 339-700, Republic of Korea

HIGHLIGHTS

- Cow dung is used as a carbon precursor, which is an abundant biological waste.
- Synthesized activated carbon has high surface area with suitable amount of mesopore.
- Inherently present inorganic and organic materials leads to high amount of pores.
- High specific capacitance along with excellent durability is achieved.
- Capacitive performance has significant dependence on mesopore–micropore ratio.

GRAPHICAL ABSTRACT



ARTICLE INFO

Article history:

Received 8 February 2014
Received in revised form
29 March 2014
Accepted 30 March 2014
Available online 4 April 2014

Keywords:

Cow dung
Activation
Supercapacitor
Organic electrolyte
Two-electrode system

ABSTRACT

Cow dung is one of the most abundant wastes generated on earth and has been traditionally used as fertilizer and fuel in most of the developing countries. In this study activated carbon is synthesized from cow dung by a modified chemical activation method, where partially carbonized cow dung is treated with KOH in different ratio. The synthesized activated carbon possesses irregular surface morphology with high surface area in the range of $1500\text{--}2000\text{ m}^2\text{ g}^{-1}$ with proper amount of micropore and mesopore volume. In particular, we demonstrate that the surface morphology and porosity parameters change with increase in KOH ratio. These activated carbons are tested as electrode material in two-electrode symmetric supercapacitor system in non-aqueous electrolyte and found to exhibit high specific capacitance with excellent retention of it at high current density and for long term operation. In particular, the activated carbon synthesized at 2:1 ratio of KOH and the pre-carbonized char shows the best performance with specific capacitance of 124 F g^{-1} at 0.1 A g^{-1} and retains up to 117 F g^{-1} at 1.0 A g^{-1} current density. The performance is attributed to high surface area along with optimum amount of micropore and mesopore volume.

© 2014 Elsevier B.V. All rights reserved.

1. Introduction

Carbon materials are used in wide range of applications depending on their electrical conductivity, polarizability, chemical

inertness and structural strength along with tuneable electrical, thermal and optical properties [1–3]. Amongst them, porous carbon materials are very popular as electrode materials for Li secondary battery, supercapacitor, dye sensitized solar cell, and fuel cell [4–11]. Porous carbon materials have been synthesized by various methods such as hard or soft sacrificial template by using silica or surfactant, catalytic activation by using metal salts or

* Corresponding author. Tel.: +82 44 860 1494; fax: +82 44 860 1331.

E-mail address: jsyu212@korea.ac.kr (J.-S. Yu).

organometallic compounds, carbonization of polymer blends and aerogel, chemical activation, physical activation, and etc [6–12]. Owing to consumption of expensive precursor, energy as well as time, development of simple low-cost strategies is still a foremost challenge for synthesis of nanostructured carbon materials [12]. Natural biomass-based organic materials, which are present ubiquitously on earth, therefore have emerged as a plausible alternative for carbon precursor. Several biomass-based materials such as rice straw, gelatin, pine needles, coffee bean, corn stalk, cow dung etc are employed to synthesize nanostructured carbon materials with high surface area and tuneable porosity [13–22]. In developing world, cow dung has been used for centuries as cooking fuel, sanitizing cleanser, construction material, insulation, and waterproofing for walls and floors in rural houses, cultural symbol in religious worship, and raw-material for producing organic composite and generating electricity. Despite of being a cheap and abundant source for synthesizing functional carbon materials, cow dung has not been explored much. Among the few reports that can be found in literature, Demiral et al. [17] have reported the synthesis of activated carbon with high surface area from cow dung using $ZnCl_2$ and KOH activation. On the other hand, Das et al. [23] have utilized activated carbon synthesized from cow dung for removal of Cr(IV) ions from water. But, to the best of our knowledge after extensive literature survey, cow dung carbon has been unexplored in any electrochemical application.

Supercapacitor, alias electrochemical capacitor is a promising candidate for high energy storage due to its outstanding advantages such as high power density (10^3 – 10^4 W kg $^{-1}$), long cycle life ($>10^6$ cycles), pulse power supply, low maintenance cost, simplicity and better safety compared to secondary batteries [1,24–27]. Electric vehicles can be considered as a platform for use of supercapacitor when high power density is needed during acceleration and the energy can be recovered during braking. Depending on mechanism of charge storage, supercapacitors can be categorized in two major classes, i.e. electrochemical double-layer capacitor (EDLC) and pseudocapacitor. The capacitance of EDLC comes from non-faradic charge accumulation at interfacial double layer of electrode and electrolyte, whereas in pseudocapacitors, reversible faradic redox reactions also add up the capacitance along with non-faradic charge [24–27]. Carbon materials with high surface areas are generally used as EDLC electrodes, while conducting polymers and metal oxides are used in construction of pseudocapacitors [26–28]. Although specific capacitance of pseudocapacitors are often better than EDLC, slow rate and probable irreversibility of faradic processes lead to degradation of performance of pseudocapacitors at higher current density and also in long term operation [25–27]. Specific surface area, pore structure of electrodes, ionic conductivity and voltage stability of electrolyte are the main factors which regulate the energy stored in EDLC [29]. High specific capacitance can be achieved in aqueous electrolyte due to their high conductivity, small ionic size and probable faradic process, but it is unfavourable to use aqueous electrolytes due to possible corrosion of current collector and smaller electrochemical window. Organic electrolytes have high potential window and also, are non-corrosive. Therefore, organic electrolytes are often utilized for getting high energy density and durability in EDLC application.

Microporous activated carbon materials are found to be usual choice as electrode materials, which deliver high capacitance and power density due to their very high surface area and pore volume as well as low cost [27–32]. Contrary to a common perception that specific capacitance is directly related to specific surface area, ultra-micropores (pore size ≤ 0.8 nm) in activated carbons are non-accessible to big organic electrolyte ions, and eventually the active electrode/electrolyte interface area is only partially realized in such system, producing lower specific capacitance than expected

[33,34]. Therefore it is necessary to have sufficient mesopore volume and their good interconnectivity for organic electrolyte to effectively reach all the available surface area in carbon framework [35–38]. Thus, an appropriate control over mesopore/micropore volume and proper choice of electrolyte is expected to be crucial to ensure a good performance of supercapacitor in terms of both power delivery rate and energy storage capacity. Alkali activation is the most effective method for synthesis of porous carbon, for which, NaOH or KOH is used most commonly and mainly results in microporous carbon materials [14,39–45]. Usually, the synthesis of activated carbons by alkali activation approach includes two steps: pyrolysis of precursors at a moderate or high temperature under inert atmosphere to obtain a carbon-enriched char, followed by high temperature pyrolysis of the char mixed with alkali to create a porous structure [46].

In this study, we have synthesized activated carbon from a cheap and abundant biological waste i.e. cow dung by using KOH as activating agent. The as-synthesized activated cow dung carbon (**ACDC**) has high amount of mesopores along with micropores formed by KOH. The inorganic materials inherently present in cow-dung is found to be responsible for formation of mesopores. As a result of optimum combination of mesopore/micropore, the **ACDC** exhibits excellent performance as electrode material for supercapacitor.

2. Experimental section

2.1. Synthesis

The activated cow dung carbon (**ACDC**) was synthesized by chemical activation method using KOH as an activating agent and pre-carbonized cow dung char as a precursor. Initially, the sun-dried cow dung was pre-carbonized at 450 °C for 2 h under constant N₂ flow. Then, the char was mixed with KOH in different proportions in minimum volume of water and stirred at 80 °C until formation of homogenous slurry. The slurry was then transferred to an alumina crucible and pyrolyzed under constant N₂ flow at 800 °C with temperature ramp rate of 10 °C min $^{-1}$ and then maintained there for 2 h before natural cooling. The obtained product was washed with 1.0 M HF to remove inorganic impurity and then with deionized water till the filtrate became neutral. The products were finally dried overnight at 80 °C. The amount of KOH to char ratio in terms of weight was varied from 1 to 3 and thus obtained carbon was designated as **ACDC-1**, **ACDC-2** and **ACDC-3**.

2.2. Surface characterization of various carbon materials

The surface morphologies of the synthesized **ACDCs** were characterized by field emission scanning electron microscopy (FE-SEM) using a Hitachi S-4700 microscope operated at an acceleration voltage of 10 kV. N₂ adsorption-desorption isotherms were measured at –196 °C on Micromeritics ASAP 2020 surface area and porosity analyzer after the carbon sample was degassed at 150 °C to 20 mTorr for 12 h. The specific surface area (S_{BET}) was determined from nitrogen adsorption in the relative pressure range from 0.05 to 0.2 using the Brunauer–Emmett–Teller (BET) equation. The total pore volume (V_{total}), micropore volume (V_{micro}) and pore size distribution were determined by density functional theory (DFT) method. Electrical resistivity of the **ACDC** samples was measured by four probe method at different pressures using a custom-made cell described in earlier work [47]. X-ray diffraction (XRD) patterns of samples were obtained using a Rigaku Smartlab diffractometer with CuK α radiation using a Ni β -filter at a scan rate of 2°/min. The X-ray source was operated at 40 kV and 30 mA.

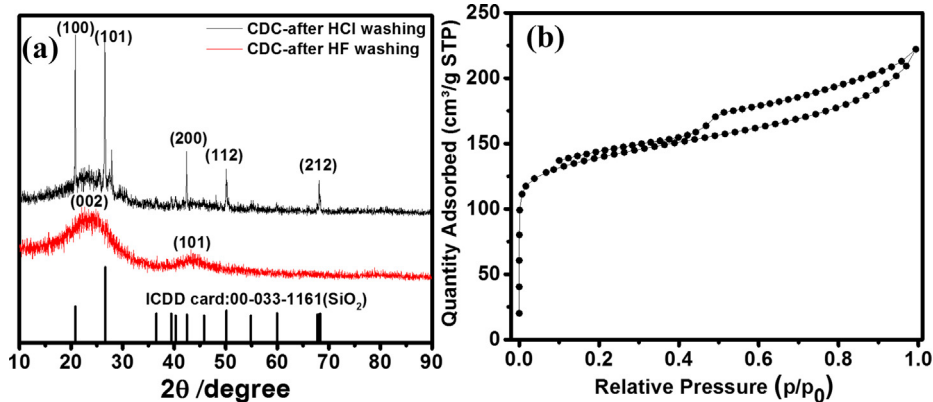


Fig. 1. (a) XRD spectra of pyrolyzed cow dung carbon after washing by 1.0 M HCl and 1.0 M HF solution. (The XRD peaks other than those of carbon are matched with quartz phase of silica) and (b) nitrogen adsorption–desorption isotherm of pyrolyzed cow dung carbon after washing by 1.0 M HF solution.

2.3. Cell construction and electrochemical measurements

All electrochemical characterizations of the synthesized **ACDCs** were performed in an electrochemical workstation (VMP3, Bio-logic) using a symmetrical two-electrode configuration with 1.0 M tetraethylammonium tetrafluoroborate (Et_4NBF_4) in acetonitrile (AN) as electrolyte. The two-electrode test cell configuration with organic electrolyte is regarded as the most reliable and practical method for evaluating a material's performance for supercapacitors [48]. All the electrode fabrication and cell construction steps were conducted in argon-filled glove box with air and moisture content below 10 ppm. The electrolyte was dried by using molecular sieves and stored in the glove box prior to use. 99.99% pure Aluminium foil with 20 μm in thickness (MTI corp.) was used to serve as a current collector. The active **ACDC** material was mixed with a conducting agent (graphite) and a binder (polyvinylidifluoride) in the weight ratio of 8:1:1, and slurry was prepared by using 1-methyl-pyrrolidone as a solvent. The slurry was casted on the Al foil in the form of

a film by using a doctor blade (Hohsen Corporation, Japan) and then dried overnight at room temperature. These dried films were then pressed by a roll press (Hohsen Corp.) to obtain 20 μm thick films and dried again in vacuum oven at 100 °C overnight. Electrodes of 2.0 cm^2 in area were cut by electrode punch (Hohsen Corp.) and used as working electrode. Approx. 4 mg of active materials was loaded in each electrode. The employed procedure was found to provide a low interface resistance between the Al current collector and the electrode. The electrodes were kept in a desiccator filled with silica gel to avoid moisture contamination while transferring to the glove box. The cell was constructed using an air-tight HS-Flat test cell (Hohsen Corp.) with two working electrodes separated by polypropylene separator (Celgard 2400) and about 200 μL electrolyte. The constructed cell was kept overnight to ensure proper wetting of electrodes by the electrolyte. The electrochemical measurements were carried out by cyclic voltammetry (CV) and galvanostatic charge–discharge (CD) and electrochemical impedance spectroscopy (EIS) methods. CV and CD were recorded in 0–

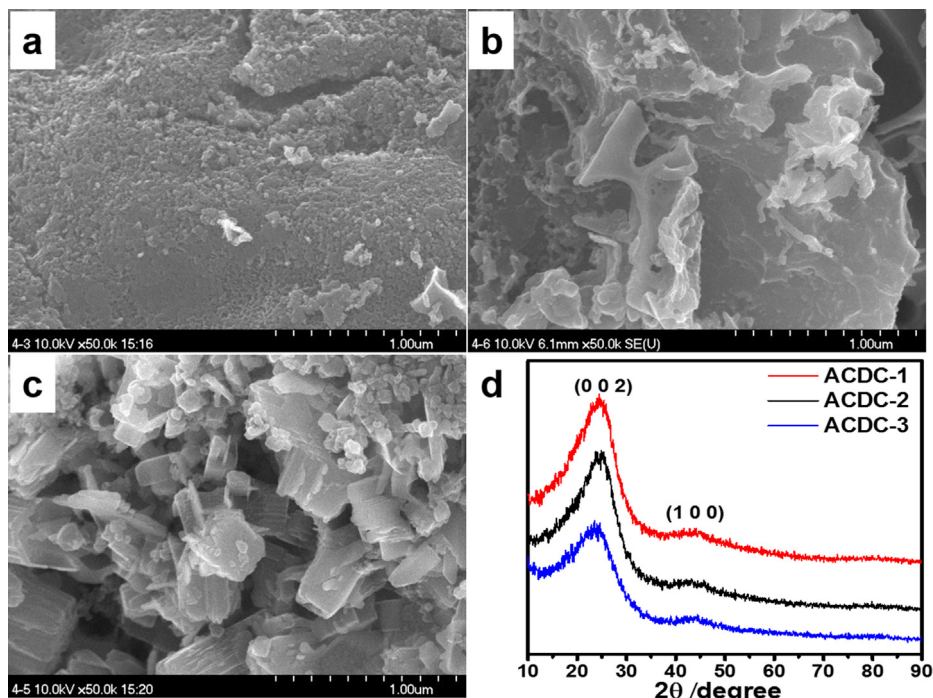


Fig. 2. FE-SEM images of (a) ACDC-1 (b) ACDC-2, and (c) ACDC-3 and (d) XRD spectra of corresponding **ACDC** samples.

2.5 V potential window. EIS measurements were carried out in the frequency range of 10 kHz to 10 mHz with a 10 mV AC amplitude around 0 V. The Nyquist plot obtained was fitted with an equivalent circuit using ZFit programme to get the impedance parameters. The specific capacitance was calculated from CV and CD measurements using the following equation:

$$C_{sp} = 2 \times I/m \times (dV/dt) \quad (1)$$

where, I is the current, m is the mass of the active material in a single electrode and (dV/dt) represents the potential scan rate in CV measurement and slope of discharge curve in CD measurement. Specific capacitance can also be calculated from EIS measurement by using the following equation:

$$C_{sp} = 1/\pi \times m \times f \times z'' \quad (2)$$

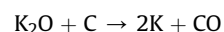
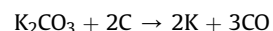
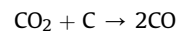
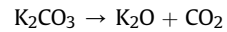
where, f is the AC frequency applied and Z'' is the imaginary part of impedance measured during EIS spectroscopy.

3. Results and discussion

Cow dung contains primarily undigested remaining of cattle feed. So it has several kinds of inorganic and organic materials (Fig. S3 and Table S1 of Electronic Supplementary material (ESM)). To know the presence of inorganic materials, the dried cow-dung was pyrolyzed at 800 °C under constant N₂ flow without using any activating agent. The product was then washed with 1.0 M HCl solution, and both precipitate and filtrate was dried. Fig. S1 of ESM shows XRD spectrum of the dried filtrate after HCl washing of pyrolyzed cow dung carbon (CDC-HCl). Electron probe microanalysis of the dried filtrate after HCl washing (see Fig. S2 of ESM) reveals the presence of various elements, which compose the inorganic materials in cow dung. The XRD spectrum in Fig. 1a shows that the CDC-HCl has quartz as impurity phase, along with obvious turbostratic disordered carbon phase. The presence of quartz is considered to be due to the silica materials present in straw-based cattle feed. After washing by 1.0 M HF, the silica was completely removed and pure turbostratic carbon phase was observed. Fig. 1b represents N₂ adsorption-desorption analysis of the CDC after HF washing, which reveals type IV isotherms with prominent H4 type hysteresis typical of mesoporous materials [30]. Removal of silica and inorganic materials from carbon framework leads to formation of mesopores and thus, the CDC has BET surface area of 521 m² g⁻¹ with 50% mesopore volume.

It is well known that high surface area is a primary requirement for getting high specific capacitance in non-aqueous electrolyte for carbon electrodes. Therefore, ACDCs, i.e. ACDC-1, ACDC-2 and ACDC-3 were synthesized by activating the pre-carbonized char at three different KOH/char ratios from 1 to 3. FE-SEM morphologies of them are shown in Fig. 2a, b and c, respectively, where highly irregular and rough surface stature originated from highly porous morphology can be observed for all the samples. But, on careful observation, we can see that the surface in ACDC-1 is rough and bulky with large particles more than 10 μm, whereas ACDC-2 shows decrease in particle size although they are still interconnected. But at KOH/char ratio of 3, ACDC-3 revealed much smaller particles of less than 1 μm in size.

Overnight stirring of char with KOH leads to a homogeneous mixture of them, and at high temperature KOH oxidatively reacts with char carbon to form H₂, CO₂ and CO gas and thus create the pores [46]. The reaction mechanism of KOH activation is followed as:



As the KOH amount increases, the amount of pores and their average size increase. However, high KOH amount leads to excessive formation of pores and finally breakage of bulky particle to smaller particles which can reduce the overall surface area as well as graphiticity. Therefore, the KOH amount should be optimized to get interconnected porous structure with proper amount of mesosized pores (pore width 2–50 nm) which are helpful for fast charge and mass transport at high current density without affecting the overall conductivity [43,49]. Fig. 2d shows the XRD spectra of all ACDC samples, where indicate turbostratic disordered carbon with low crystallinity between graphite and amorphous carbon. The peak at 26.3° is related to (002) graphitic plane, presence of which indirectly ensures the presence of in-plane conductivity required for electrochemical application. On careful observation, decrease in crystallinity can be readily observed with broadening of graphitic peak for ACDC-3.

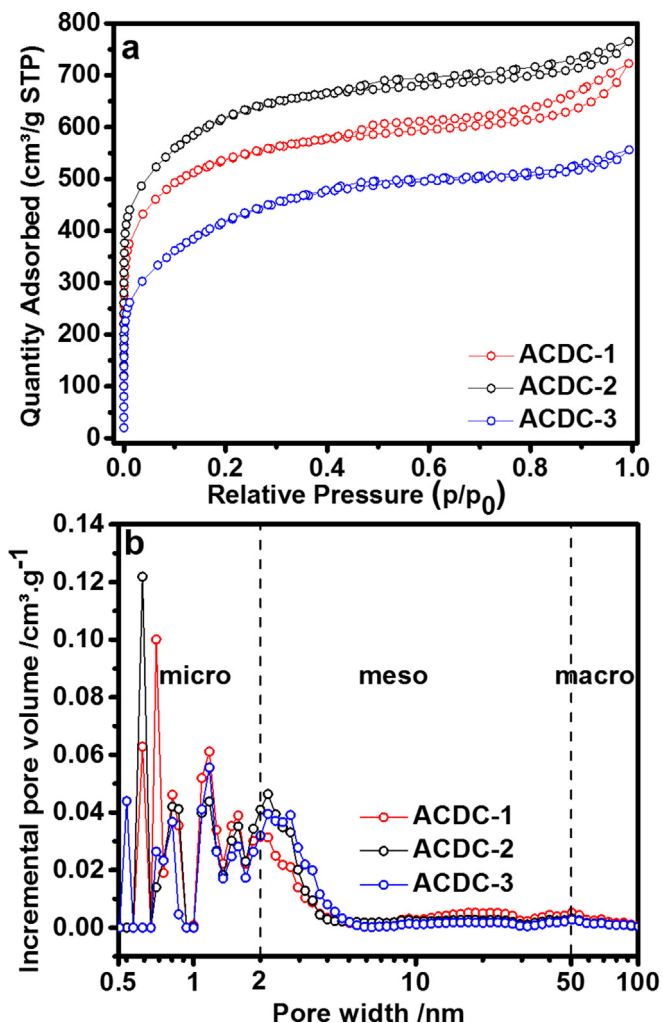


Fig. 3. (a) Nitrogen adsorption–desorption isotherms and (b) DFT pore size distribution (PSD) profiles of ACDC samples.

Table 1Porosity parameters of **ACDCs** obtained from BET analysis.

	$S_{\text{BET}}^{\text{a}}$ ($\text{m}^2 \text{ g}^{-1}$)	V_T^{b} ($\text{cm}^3 \text{ g}^{-1}$)	$V_{\text{micro}}^{\text{c}}$ ($\text{cm}^3 \text{ g}^{-1}$)	% of V_{micro}
CDC	521	0.26	0.13	50
ACDC-1	1858	0.81	0.54	67
ACDC-2	1984	0.91	0.62	68
ACDC-3	1510	0.70	0.40	57

^a S_{BET} : BET surface area.^b V_T : total pore volume measured from DFT analysis (between 0.46 nm and 172 nm pore size).^c V_{micro} : micropore volume (below 2 nm pore size).

Fig. 3 shows N_2 adsorption–desorption analysis of the synthesized activated carbons. All the profiles in **Fig. 3a** reveal similar type I isotherms with small H4 type hysteresis, which is characteristic of microporous materials with high amount of mesopore volume. **Table 1** displays the porosity data obtained from N_2 sorption isotherm analysis. It can be observed that **ACDC-2**, synthesized at KOH/char ratio of 2, has the highest BET surface area with highest micropore volume, whereas **ACDC-1** has slightly lower BET surface area with lower micropores, and **ACDC-3**, synthesized at KOH/char ratio of 3 reveals the lowest BET surface area with lowest micropore volume. The DFT pore size distribution in **Fig. 3b** shows higher amount of pores in both microporous and mesoporous region for **ACDC-2**. Interestingly, all the prepared carbon samples reveal almost identical mesopore volume of $0.27\text{--}0.30 \text{ cm}^3 \text{ g}^{-1}$. Cow dung contains undigested remaining of cattle feed and therefore contains lots of inorganic non-volatile materials (see **Figs. S1, S2, S3** and **Table S1** of ESM) and/or thermally unstable organic impurities. Due to high temperature treatment followed by washing with 1.0 M HF solution during activation, the impurities were removed from the carbonaceous materials leaving behind abundant pores in **ACDC** along with pores created by KOH activation. Since chemical

activation generally leads to micropores in carbon surface, the formation of high amount of mesopores in all the carbon samples can be mainly attributed to removal of inorganic materials present in cow dung, which is supposed to be identical for all the samples. Therefore, at optimum ratio of KOH/char, the surface area and pore volume are of maximum, which is achieved at KOH/char ratio of 2. But at high KOH/char ratio of 3, excessive burn-off of carbon surface takes place, which leads to breakage in carbon structure, and thereby both surface area and pore volume decrease substantially.

To evaluate the characteristics of the as-synthesized activated carbons as electrode materials for supercapacitors, they were tested in symmetric two-electrode system using non-aqueous electrolyte simulating commercial EDLC. Such system is found to provide more reliable and practical data for evaluating a material's performance for supercapacitors. **Fig. 4a** shows the comparative cyclic voltammograms of all **ACDC** samples at 10 mV s^{-1} potential scan rate. The cyclic voltammetry (CV) profiles obtained for **ACDC-1** and **ACDC-2** are symmetric and rectangular in shape, typically being shown by EDLC with negligible internal cell resistance. **ACDC-3** shows relatively high internal cell resistance, as evidenced by shifting from vertical change in current density on altering the electrode polarity near at 0 V and 2.5 V. It may be caused by increase in electrical resistivity in **ACDC-3** (**Fig. S4** of ESM) due to severe loss of structural connectivity caused by excessive activation. This is evident from substantial decrease in relative percentage of micropores in BET analysis and broken morphology in SEM analysis. There is a small amount of faradic movement from 2.0 V to 2.5 V for all the samples, which may be due to decomposition of residual moisture in electrode and/or electrolyte. **ACDC-2** shows the best performance in terms of specific capacitance among all the prepared samples due to its highest surface area and also probably due to suitable amount of micropore and mesopore volume, which plays an important role in EDLC performance. Although mesopores

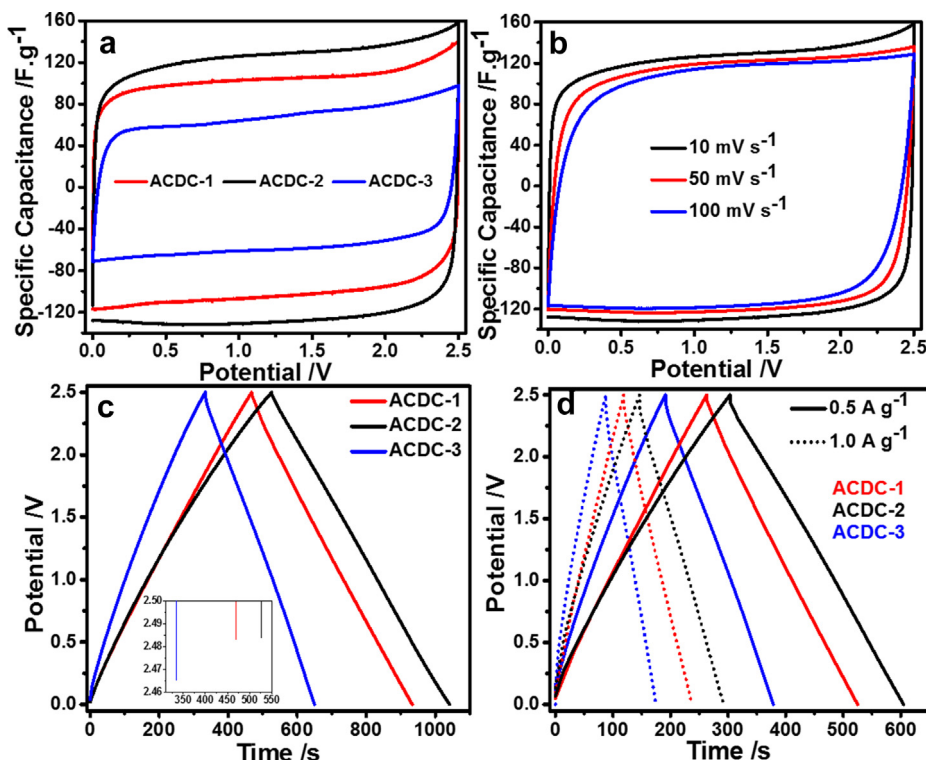


Fig. 4. Comparative cyclic voltammograms of (a) all **ACDCs** at 10 mV s^{-1} potential scan rate and (b) **ACDC-2** at different potential scan rate. Galvanostatic charge-discharge profiles of all the **ACDCs** (c) at 0.3 A g^{-1} with inset showing IR drop and (d) at 0.5 A g^{-1} and 1.0 A g^{-1} .

themselves can play limited role in storing charges, they can allow bulky organic electrolyte ions to make facile movement and thus to effectively access active surfaces present in micropores. So, optimum amount of both micropores and mesopores is necessary for getting high electrochemical performance. In Fig. 4b, it can be seen that the rectangular CV shape of **ACDC-2** is also maintained superbly at higher potential scan rates of 50 mV s^{-1} and 100 mV s^{-1} , which may be attributed to the optimum amount of combined micropore and mesopore volume as well as good electrical conductivity [36].

Fig. 4c shows the typical galvanostatic charge–discharge (CD) profiles of the as-prepared activated carbons at 0.3 A g^{-1} current density. All of them show perfect isosceles triangular CD behaviour ideal to EDLC. **ACDC-1** and **ACDC-2** show less iR drop than **ACDC-3**. **ACDC-2** shows highest specific capacitance of 125 F g^{-1} at 0.3 A g^{-1} . High specific capacitance of **ACDC-2** can be attributed not only to the highest surface area, but also to the more favourable amount of micropore and mesopore. **ACDC-1** has slightly lower specific capacitance of 112 F g^{-1} due to less surface area and less micropore volume. However **ACDC-3** shows significantly less specific capacitance of 80 F g^{-1} due to substantially less surface area along with even lower percentage of micropore volume. These are caused by excessive burn off of carbon networks leading to breakage into smaller particles with excessive amount of KOH, resulting in decrease in amount of active surface for charge storage and increase in electrical resistivity (see Fig. S4 of ESM). The decrease in crystallinity is also evident from broadening of graphitic peak for **ACDC-3** in Fig. 2d, which is in consistent with increase in electrical resistivity. Overall, all of the **ACDCs** have demonstrated higher specific capacitance than 62 F g^{-1} of commercial activated carbon (Norit A supra) tested in our laboratory in the same testing conditions [36]. Even though Norit A supra has higher surface area of

$2170 \text{ m}^2 \text{ g}^{-1}$, the mesopore volume is very low (ca. 10% of total pore volume of $1.07 \text{ cm}^3 \text{ g}^{-1}$), which restrict the organic electrolyte ions to access all of the active surfaces. Fig. 4d shows CD profiles of **ACDCs** at higher current density of 0.5 A g^{-1} and 1.0 A g^{-1} . It can be readily seen that IR drop increases at higher current density, but this increase is more prominent in **ACDC-3** than the other two. Lower increase in IR drop at higher current density means lower dissipation of capacitance in terms of heat. More favourable combination of micropores and mesopores in **ACDC-2** and **ACDC-1** ensures higher intrinsic conductivity and thereby results in higher capacitance retention at high current density as compared to **ACDC-3**. Therefore **ACDC-1**, **ACDC-2** and **ACDC-3** could be able to deliver 121 , 105 and 72 F g^{-1} at 0.5 A g^{-1} current density and 117 , 99 and 65 F g^{-1} at 1.0 A g^{-1} current density, respectively. The behaviour also emphasizes the importance of mesopores in ion transport as well as of micropores in charge storage. High potential window of the organic electrolyte implies a high energy density according to $E = (1/2)C_{\text{cell}}V^2$, where C_{cell} is total capacitance of the cell (which is a quarter of the specific capacitance of electrode calculated by Equation (1)) and V is the voltage. The calculated energy density of the cells made from **ACDC-1** and **ACDC-2** are calculated to be 24 and 28 W h kg^{-1} at 1 A g^{-1} current density, which are among the excellent values reported for porous carbon materials and in the range of Ni–MH battery. [22,30,50–56].

High durability is a highly required parameter for electrode materials to endure good structural integrity over long term operation. To check this performance, all of the **ACDC** electrodes were tested for 1000 cycles of galvanostatic CD at 1.0 A g^{-1} current density. Fig. 5a shows that all of the **ACDC** samples have retained over 85% of initial capacitance up to 1000 CD cycles and have similar decrease behaviour. Electrochemical impedance spectroscopy (EIS) is another important tool for checking different kinds of

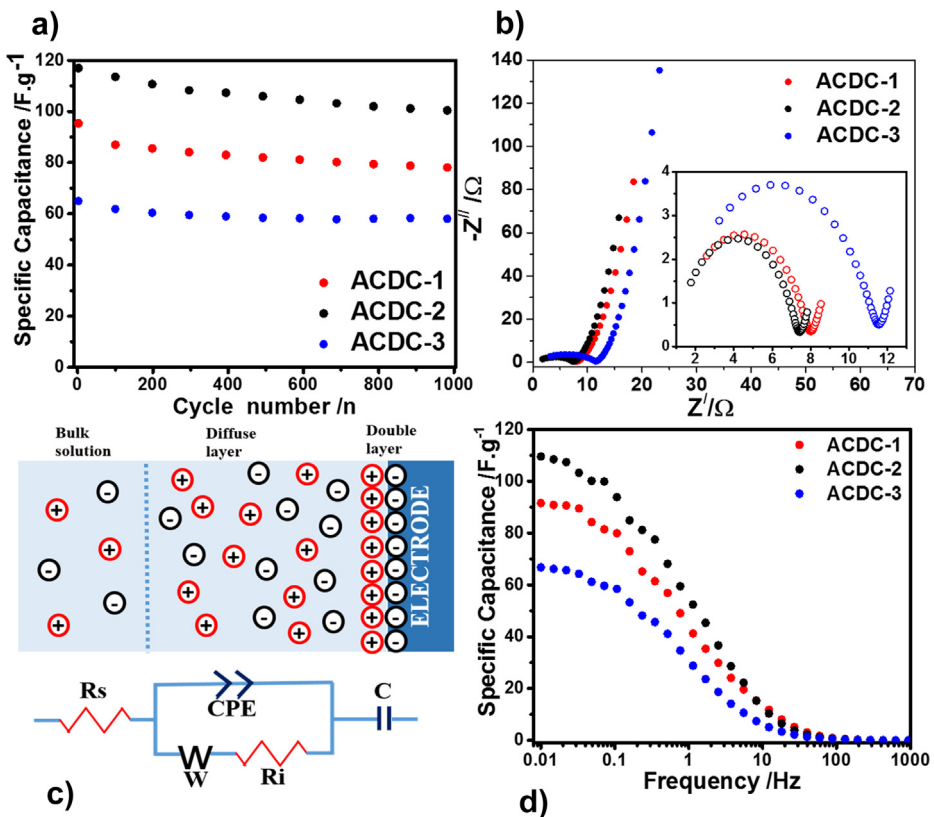


Fig. 5. (a) Cyclic performance and (b) Nyquist impedance plots for the prepared **ACDCs**, (c) equivalent circuit model used for fitting and (d) variation of specific capacitance with frequency for the **ACDCs**.

Table 2EIS parameters of **ACDCs** obtained from analysis of Nyquist plot.

	R_s (Ω)	CPE ($\text{mF s}^{1/\alpha}$)	R_i (Ω)	W ($\Omega \text{ s}^{-1/2}$)	C (mF)
ACDC-1	0.94	0.04 ($\alpha = 0.81$)	6.94	2.65	218
ACDC-2	0.95	0.05 ($\alpha = 0.84$)	6.35	2.12	272
ACDC-3	0.81	0.04 ($\alpha = 0.78$)	10.52	2.96	129

resistive phenomenon associated with electrochemical energy storage [57,58]. In this technique, alternating current of low amplitude is applied at open circuit potential to investigate penetration ability of ions through the porous network of the electrode at different frequency. The results of EIS measurements performed for our samples are represented by Nyquist plots in Fig. 5b. All of the **ACDCs** show a well-defined semicircle in the high to medium frequency regions and nearly vertical line in the low frequency region. All of the Nyquist plots are fitted to an electrical circuit reported by Hung et al. with minor modification [53]. Similar circuit models are also presented by Wang et al. and Fabio et al. [59,60]. The Circuit model is shown in Fig. 5c and starts from bulk of the electrolyte to electrode surface through an electrical double layer [61]. The electrical double layer in the pores of ACDC electrodes are formed by the electrolyte ions diffusing towards the Helmholtz plane inside the pores [53]. The starting point of the semicircle in the real axis of the Nyquist spectrum generated in high frequency region is solution resistance (R_s), which occurs due to ionic conductivity of the electrolyte ions. It is followed by a semicircle in the high to medium frequency region formed by the diffusion layer. This region is governed by ability of ion migration through the pores and electrical resistivity of the electrode material. This diffusion layer consists of a parallel combination of constant phase element (CPE) and a series of interface resistance (R_i) and Warburg resistance (W). CPE is an imperfect capacitance of the diffusion layer with α as degree of deviation ($\alpha = 1$ for ideal capacitor and 0 for ideal resistor), which is related to the capacitance developed in the diffusion layer. R_i is interface resistance created on the diffusion layer, which significantly affect the IR drop and rate capability of the cell, while W represents the hindrance in electrolyte diffusion through porous network of the electrode. [22,60] The straight line in low frequency region of Nyquist plot is the double layer capacitance (C) generated at the electrode surface i.e. Helmholtz plane. In this low frequency region, slow charge–discharge process allows the electrolyte ions to have enough time to move from diffusion layer to Helmholtz plane [53]. The results obtained by the analysis of the Nyquist plots are summarized in Table 2. It can be seen that R_s values are almost similar in the range of 0.81–0.95 for all the samples since similar condition was maintained during all the cell preparations. The interface resistance (R_i) is similar in **ACDC-1** and **ACDC-2**, but is higher in case of **ACDC-3**. This can be explained by the increase in electrical resistivity of **ACDC-3**, which is also supported by CV and CD behaviour. The Warburg resistance is lowest in **ACDC-2** followed by a little increase in **ACDC-1** and **ACDC-3**. The double layer capacitance follows the trend shown by CV and CD behaviour, i.e. **ACDC-2** shows highest double layer capacitance followed by **ACDC-1** and **ACDC-3**. Fig. 5d shows the variation of specific capacitance with applied frequency. This frequency-depended capacitance can be directly correlated to the rate capability of the cell. Here also it is observed that **ACDC-2** not only shows highest specific capacitance at low frequency, but also retains 50% of capacitance up to 1 Hz. This behaviour is in accordance with the results of CV and CD measurements. Overall, all of the **ACDCs** show impressive performance as electrode for supercapacitor and hold high potential for commercialization as the precursor is cheap and synthesis method is very simple.

4. Conclusions

This study manifests an easy and efficient conversion of a biological waste material to a value-added material. Activated carbon samples with high surface area and proper amount of micropores and mesopore volume were synthesized from biological waste cow dung. The synthesis method involves treatment of pre-carbonized char with different ratios of KOH and pyrolysis at 800 °C followed by HF washing. The obtained activated carbons were tested as supercapacitor electrodes in practical Two-electrode symmetric system using non-aqueous electrolyte. To the best of our knowledge, this is the first report on use of the porous carbon made from cow dung in any kind of electrochemical application. All the activated carbons showed excellent performance in terms of specific capacitance and durability at high current density and for long term operation. The activated carbon synthesized at 2:1 ratio of KOH and the pre-carbonized char has shown the best performance with specific capacitance of 124 F g⁻¹ at 0.1 A g⁻¹ and retained up to 117 F g⁻¹ at 1.0 A g⁻¹ current density. The performance was attributed to high surface area along with optimum amount of micropore and mesopore volume. While micropores contribute to the specific capacitance value, mesopores allow big non-aqueous electrolyte ions to make efficient movement and thus to reach maximum surface area. Further increase in KOH amount led to decrease in micropore volume and disintegration of continuous pore network, and as a result, decrease in intrinsic conductivity, which reduce the overall EDLC performance. All of the results demonstrate that highly porous activated carbon can be easily synthesized from biological waste cow dung for commercial use as electrode materials for supercapacitor. Further studies are going on for using the electrode materials for other energy storage and conversion system such as Li-ion batteries and fuel cells.

Acknowledgements

This work was supported by NRF grant (NRF 2010-0029245) and Global Frontier R&D Program on Center for Multiscale Energy System (NRF 2011-0031571) funded by the Ministry of Education, Science and Technology through the National Research Foundation of Korea. The authors also would like to thank Dana Kim and Nitin Chaudhari for providing the cow dung, and Hyeon-yeol Park and Jong-deok Park for FE-SEM and BET analysis.

Appendix A. Supplementary data

Supplementary data related to this article can be found at <http://dx.doi.org/10.1016/j.jpowsour.2014.03.143>.

References

- [1] E. Frackowiak, F. Béguin, Carbon 39 (2001) 937–950.
- [2] K. Kinoshita, Carbon: Electrochemical and Physicochemical Properties, 1988.
- [3] B. Fang, J.H. Kim, M.-S. Kim, J.-S. Yu, Acc. Chem. Res. 46 (2012) 1397–1406.
- [4] S.L. Candelaria, Y. Shao, W. Zhou, X. Li, J. Xiao, J.-G. Zhang, Y. Wang, J. Liu, J. Li, G. Cao, Nano Energy 1 (2012) 195–220.
- [5] M. Srivastava, M. Kumar, R. Singh, U. Agrawal, M. Garg, J. Sci. Ind. Res. 68 (2009) 93–96.
- [6] D.-S. Yang, D. Bhattacharjya, S. Inamdar, J. Park, J.-S. Yu, J. Am. Chem. Soc. 134 (2012) 16127–16130.
- [7] S. Inamdar, H.-S. Choi, P. Wang, M.Y. Song, J.-S. Yu, Electrochim. Commun. 0 (2013) 9–12.
- [8] B. Fang, J.H. Kim, M. Kim, J.-S. Yu, Chem. Mater. 21 (2009) 789–796.
- [9] D. Bhattacharjya, H.-Y. Park, M.-S. Kim, H.-S. Choi, S.N. Inamdar, J.-S. Yu, Langmuir 30 (2013) 318–324.
- [10] J.H. Kim, B. Fang, M.Y. Song, J.-S. Yu, Chem. Mater. 24 (2012) 2256–2264.
- [11] D.-S. Yang, D. Bhattacharjya, M.Y. Song, J.-S. Yu, Carbon 67 (2014) 736–743.
- [12] J. Lee, J. Kim, T. Hyeon, Adv. Mater. 18 (2006) 2073–2094.
- [13] B. Hu, K. Wang, L. Wu, S.-H. Yu, M. Antonietti, M.-M. Titirici, Adv. Mater. 22 (2010) 813–828.

[14] B. Xu, S. Hou, G. Cao, F. Wu, Y. Yang, *J. Mater. Chem.* 22 (2012) 19088–19093.

[15] X. Li, C. Han, X. Chen, C. Shi, *Microporous Mesoporous Mater.* 131 (2010) 303–309.

[16] X. Li, W. Xing, S. Zhuo, J. Zhou, F. Li, S.-Z. Qiao, G.-Q. Lu, *Bioresour. Technol.* 102 (2011) 1118–1123.

[17] H. Demiral, İ. Demiral, *Surf. Interface Anal.* 40 (2008) 612–615.

[18] L. Wei, M. Sevilla, A.B. Fuertes, R. Mokaya, G. Yushin, *Adv. Energy Mater.* 1 (2011) 356–361.

[19] M. Biswal, A. Banerjee, M. Deo, S. Ogale, *Energy Environ. Sci.* 6 (2013) 1249–1259.

[20] C. Falco, J.M. Sieben, N. Brun, M. Sevilla, T. van der Maelen, E. Morallón, D. Cazorla-Amorós, M.-M. Titirici, *ChemSusChem* 6 (2013) 374–382.

[21] C. Huang, T. Sun, D. Hulicova-Jurcakova, *ChemSusChem* 6 (2013) 2330–2339.

[22] L. Wang, G. Mu, C. Tian, L. Sun, W. Zhou, P. Yu, J. Yin, H. Fu, *ChemSusChem* 6 (2013) 880–889.

[23] D.D. Das, R. Mahapatra, J. Pradhan, S.N. Das, R.S. Thakur, *J. Colloid Interface Sci.* 232 (2000) 235–240.

[24] M. Lu, F. Beguin, E. Frackowiak, *Supercapacitors: Materials, Systems and Applications*, Wiley, 2013.

[25] A.S. Arico, P. Bruce, B. Scrosati, J.-M. Tarascon, W. van Schalkwijk, *Nat. Mater.* 4 (2005) 366–377.

[26] P. Simon, Y. Gogotsi, *Nat. Mater.* 7 (2008) 845–854.

[27] G. Wang, L. Zhang, J. Zhang, *Chem. Soc. Rev.* 41 (2012) 797–828.

[28] L.L. Zhang, X.S. Zhao, *Chem. Soc. Rev.* 38 (2009) 2520–2531.

[29] R. Kötz, M. Carlen, *Electrochim. Acta* 45 (2000) 2483–2498.

[30] Y. Zhai, Y. Dou, D. Zhao, P.F. Fulvio, R.T. Mayes, S. Dai, *Adv. Mater.* 23 (2011) 4828–4850.

[31] E. Frackowiak, *Phys. Chem. Chem. Phys.* 9 (2007) 1774–1785.

[32] D. Qu, H. Shi, *J. Power Sources* 74 (1998) 99–107.

[33] A.G. Pandolfo, A.F. Hollenkamp, *J. Power Sources* 157 (2006) 11–27.

[34] J.W. Graydon, M. Panjehshahi, D.W. Kirk, *J. Power Sources* 245 (2014) 822–829.

[35] C. John, L. Celine, T. Pierre-Louis, S. Patrice, G. Yury, *Angew. Chem. Int. Ed.* 47 (2008) 3392–3395.

[36] D. Bhattacharjya, M.-S. Kim, T.-S. Bae, J.-S. Yu, *J. Power Sources* 244 (2013) 799–805.

[37] B. Fang, A. Bonakdarpour, M.-S. Kim, J.H. Kim, D.P. Wilkinson, J.-S. Yu, *Microporous Mesoporous Mater.* 182 (2013) 1–7.

[38] B. Fang, J.H. Kim, M.-S. Kim, A. Bonakdarpour, A. Lam, D.P. Wilkinson, J.-S. Yu, *J. Mater. Chem.* 22 (2012) 19031.

[39] B. Xu, S. Hou, G. Cao, M. Chu, Y. Yang, *RSC Adv.* 3 (2013) 17500–17506.

[40] L. Qie, W. Chen, H. Xu, X. Xiong, Y. Jiang, F. Zou, X. Hu, Y. Xin, Z. Zhang, Y. Huang, *Energy Environ. Sci.* 6 (2013) 2497–2504.

[41] W.M. Qiao, S.H. Yoon, I. Mochida, *Energy Fuels* 20 (2006) 1680–1684.

[42] Y. Lv, F. Zhang, Y. Dou, Y. Zhai, J. Wang, H. Liu, Y. Xia, B. Tu, D. Zhao, *J. Mater. Chem.* 22 (2012) 93–99.

[43] X. He, Y. Geng, J. Qiu, M. Zheng, X. Zhang, H. Shui, *Energy Fuels* 24 (2010) 3603–3609.

[44] B. Xu, F. Wu, Y. Su, G. Cao, S. Chen, Z. Zhou, Y. Yang, *Electrochim. Acta* 53 (2008) 7730–7735.

[45] A. Stein, Z. Wang, M.A. Fierke, *Adv. Mater.* 21 (2009) 265–293.

[46] J. Wang, S. Kaskel, *J. Mater. Chem.* 22 (2012) 23710–23725.

[47] D.-S. Yang, S. Chaudhari, K. P. Rajesh, J.-S. Yu, *ChemCatChem*, <http://dx.doi.org/10.1002/cctc.201400035>.

[48] M.D. Stoller, R.S. Ruoff, *Energy Environ. Sci.* 3 (2010) 1294–1301.

[49] V. Ruiz, A.G. Pandolfo, *J. Power Sources* 196 (2011) 7816–7822.

[50] D. Zhai, B. Li, F. Kang, H. Du, C. Xu, *Microporous Mesoporous Mater.* 130 (2010) 224–228.

[51] M. Olivares-Marín, J.A. Fernández, M.J. Lázaro, C. Fernández-González, A. Macías-García, V. Gómez-Serrano, F. Stoeckli, T.A. Centeno, *Mater. Chem. Phys.* 114 (2009) 323–327.

[52] B. Batalla García, A.M. Feaver, Q. Zhang, R.D. Champion, G. Cao, T.T. Fister, K.P. Nagle, G.T. Seidler, *J. Appl. Phys.* 104 (2008).

[53] K. Hung, C. Masarapu, T. Ko, B. Wei, *J. Power Sources* 193 (2009) 944–949.

[54] Z. Zheng, Q. Gao, *J. Power Sources* 196 (2011) 1615–1619.

[55] R.-W. Fu, Z.-H. Li, Y.-R. Liang, F. Li, F. Xu, D.-C. Wu, *New Carbon Mater.* 26 (2011) 171–179.

[56] M. Anouti, E. Couadou, L. Timperman, H. Galiano, *Electrochim. Acta* 64 (2012) 110–117.

[57] P.L. Taberna, P. Simon, J.F. Fauvarque, *J. Electrochem. Soc.* 150 (2003) A292–A300.

[58] M.E. Orazem, B. Tribollet, *Electrical Circuits*, in: *Electrochemical Impedance Spectroscopy*, John Wiley & Sons, Inc., 2008, pp. 61–72.

[59] A. Di Fabio, A. Giorgi, M. Mastragostino, F. Soavi, *J. Electrochem. Soc.* 148 (2001) A845–A850.

[60] K.-P. Wang, H. Teng, *J. Electrochem. Soc.* 154 (2007) A993–A998.

[61] X. Luo, J.J. Davis, *Chem. Soc. Rev.* 42 (2013) 5944–5962.